# Journal of Materials Chemistry B



**View Article Online PAPER** 



Cite this: J. Mater. Chem. B, 2017, **5**, 6657

## Length-dependent intracellular bundling of single-walled carbon nanotubes influences retention†

Sumin Jin, (1) ‡a Piyumi Wijesekara, (1) ‡b Patrick D. Boyer, ‡c Kris Noel Dahl (1) \*c and Mohammad F. Islam \*\*

Single-walled carbon nanotubes (SWCNTs) are increasingly being investigated for biomedical imaging, sensing, and drug delivery. Cell types, cellular entry mechanisms, and SWCNT lengths dictate SWCNT uptake, subsequent intracellular trafficking, and retention. Specialized immune cells known as macrophages are capable of two size-dependent entry mechanisms: endocytosis of small particles (diameter < 200 nm) and phagocytosis of large particles (diameter > 500 nm). In comparison, fibroblasts uptake particles predominantly through endocytosis. We report dependence of cellular processing including uptake, subcellular distribution, and retention on the SWCNT length and immune cell-specific processes. We chose SWCNTs of three different average lengths: 50 nm (ultrashort, US), 150 nm (short) and 500 nm (long) to encompass two different entry mechanisms, and noncovalently dispersed them in water, cell culture media, and phosphate buffer (pH 5) with bovine serum albumin, which maintains the SWCNT optical properties and promotes their cellular uptake. Using confocal Raman imaging and spectroscopy, we quantified cellular uptake, tracked the intracellular dispersion state (i.e., individualized versus bundled), and monitored recovery as a function of SWCNT lengths in macrophages. Cellular uptake of SWCNTs increases with decreasing SWCNT length. Interestingly, short-SWCNTs become highly bundled in concentrated phase dense regions of macrophages after uptake and most of these SWCNTs are retained for at least 24 h. On the other hand, both US- and long-SWCNTs remain largely individualized after uptake into macrophages and are lost over a similar elapsed time. After uptake into fibroblasts, however, short-SWCNTs remain individualized and are exocytosed over 24 h. We hypothesize that aggregation of SWCNTs within macrophages but not fibroblasts may facilitate the retention of SWCNTs within the former cell type. Furthermore, the differential lengthdependent cellular processing suggests potential applications of macrophages as live cell carriers of SWCNTs into tumors and regions of inflammation for therapy and imaging.

Received 17th March 2017, Accepted 14th June 2017

DOI: 10.1039/c7tb00735c

rsc li/materials-b

## Introduction

Single-walled carbon nanotubes (SWCNTs) have received much attention in cellular imaging, diagnostics, and therapy due to their high cellular uptake with almost no change in cell viability and functions. 1-3 Uptake and subcellular compartmentalization of SWCNTs in various cell lines have extensively been studied.<sup>4-6</sup> Immune cells, particularly macrophages, have emerged as attractive targets for nanoparticles and SWCNTs since these cell types are involved in many physiological and pathological conditions including wound healing, inflammation, and cancer,<sup>7,8</sup> motivating tracking of macrophages for diagnosis and altering them for therapies. 9,10 Furthermore, because macrophages are scavenger cells, they take up more SWCNTs than other cell types.<sup>5,11-15</sup> Consequently, the subcellular distribution, functional state, and residence time of SWCNTs in macrophages are important parameters to establish further applications in biomedicine.

The specific subcellular trafficking and ultimate fate of internalized nanoparticles are largely determined by the cell type<sup>1,6</sup> and the mechanism of cellular entry<sup>16,17</sup> as well as the nanoparticle surface properties 18-20 and the nanoparticle size. 21-27 Macrophages have been previously studied to explore the effect of the SWCNT physicochemical properties on cellular functions. 12,13,18-20 For example, acid-functionalization and

<sup>&</sup>lt;sup>a</sup> Department of Materials Science and Engineering, Carnegie Mellon University, 5000 Forbes Avenue, Pittsburgh, Pennsylvania 15213-3815, USA. E-mail: mohammad@cmu.edu

<sup>&</sup>lt;sup>b</sup> Department of Biomedical Engineering, Carnegie Mellon University, 5000 Forbes Avenue, Pittsburgh, Pennsylvania 15213-3815, USA

<sup>&</sup>lt;sup>c</sup> Department of Chemical Engineering, Carnegie Mellon University, 5000 Forbes Avenue, Pittsburgh, Pennsylvania 15213-3815, USA. E-mail: krisdahl@cmu.edu

<sup>†</sup> Electronic supplementary information (ESI) available. See DOI: 10.1039/c7tb00735c ‡ These authors contributed equally.

metallic impurities of SWCNTs induced increased necrosis and altered gene expression resulting in reduced phagocytic activity in macrophage cell lines, alveolar macrophages, and human monocyte-derived macrophages. 18-20,28,29 Furthermore, SWCNTs with an average length of around 3 µm and dispersed with bovine serum albumin (BSA) were found to affect the cell morphology, viability, and function with increased necrosis above a concentration of 10 µg mL<sup>-1</sup> in J774A.1 macrophages.<sup>5</sup> In contrast, ammonium functionalized and polyethylene glycol stabilized SWCNTs did not affect functional activities of immune cells. 12 Additionally, Pluronic F108 dispersed SWCNTs with a length of 1 µm were highly ingested by macrophages without showing cytotoxicity.30 In vivo administration of SWCNTs to mice, both orally and intraperitoneally, showed that individual SWCNTs of lengths less than 80 nm aggregated into sizes of lengths smaller than 2 µm and accumulated within liver and splenic macrophages.<sup>26</sup> Moreover, aggregated SWCNTs remained in murine myoblast stem cells even after 3 months. 31 In comparison, endocytosis rates of SWCNTs in many other cell types including fibroblasts increased with a decrease in the SWCNT length, but many of these SWCNTs were then lost by exocytosis. 22,23,32 Therefore, it is still unclear how the physical properties of SWCNTs and cell-specific processing affect the subcellular distribution and importantly the dispersion state of SWCNTs (i.e., individualized versus bundled) within macrophages as well as the ability of cells to expel SWCNTs and recover from exposure.

Herein, we report length-dependent uptake, subcellular distribution, and retention of SWCNTs in macrophages and compare such processing in fibroblasts to elucidate the effects of immune cellspecific processes. Macrophages are capable of two size-dependent entry mechanisms: endocytosis of small particles (diameter < 200 nm) and specialized phagocytosis of large particles (diameter > 500 nm). To maintain the optical properties of SWCNTs and promote cellular uptake into macrophages, we non-covalently disperse long-, short- and ultrashort (US)-SWCNTs of average lengths of 500 nm, 150 nm, and 50 nm, respectively, with BSA. 1,11,32-34 In our previous studies, BSA coated SWCNTs have shown homogeneous uptake in both J774A.1 macrophages and NIH-3T3 fibroblasts compared to other dispersing agents, including Pluronic F127, lysozyme, and  $\gamma$ -globulin, without causing any cytotoxic effect. 2,11,32,33,35 Using confocal Raman spectroscopy, we quantify cellular uptake, the intracellular distribution and the dispersion state of SWCNTs, and recovery from SWCNT exposure for at least 24 h in macrophages as a function of SWCNT length. We also compare cellular processing of short-SWCNTs in macrophages with that in fibroblasts to distinguish cell type dependent cellular processing. Our results on differential length-dependent cellular processing will accelerate potential applications of macrophages as live cell carriers of SWCNTs into tumors and regions of inflammation for therapy and imaging.

## Experimental

#### Preparation of SWCNT dispersions

Long-SWCNTs-BSA dispersions were prepared from raw high pressure carbon monoxide conversion synthesis (HiPCO)

SWCNTs (Carbon Nanotechnologies, Inc.) with diameters of  $1 \pm 0.3$  nm and polydisperse lengths much longer than 500 nm. To preserve the lengths of longer SWCNTs, we followed a previously reported dispersion technique that retained SWCNTs with lengths greater than 1 µm in dispersion, albeit with a different surfactant.<sup>36</sup> Briefly, ~2.2 mg of the SWCNT powder was dissolved in 2.2 mL of 10 wt% BSA (Sigma-Aldrich) solution in ultrapure deionized water (resistivity 18.3 M $\Omega$  cm, total oxidizable carbon <5 ppb) and exposed to 30 min of low power, high frequency (12 W, 55 kHz) bath sonication (Cole-Palmer Ultrasonic Cleaner). Long-SWCNTs-BSA suspensions were centrifuged for 30 min at 10 000  $\times$  g to remove large SWCNT aggregates and the supernatant was collected.

Short-SWCNTs-BSA dispersions were prepared using purified and length fractionated SWCNTs from the same HiPCO batch. The purification and length fractionation procedures, described previously in greater details, 21,37-41 resulted in a SWCNT sample containing <5 wt% carbonaceous impurities and ∼0.3 wt% metallic impurities 38,40 with lengths of 145  $\pm$  17 nm. 21,37,39,41 Short-SWCNTs were dispersed at 0.1 wt% in 1.0 wt% BSA solution in ultrapure deionized water via high power, low frequency probe-tip sonication (ThermoFisher, Model 100; 3 mm tip diameter) at 6 W for 2 h. Under these conditions, the SWCNTs are not expected to be shortened from sonication induced scission. 42 To separate bundles from isolated SWCNTs, suspensions were centrifuged at 21 000  $\times$  g for 7 min and the supernatant was collected.

US-SWCNTs were prepared via acid-cutting of raw HiPCO SWCNTs following a previously reported method.<sup>43</sup> Briefly, ~1.5 g of raw HiPCO SWCNTs were stirred at 300 rpm in 120 mL of 3:1 H<sub>2</sub>SO<sub>4</sub>/HNO<sub>3</sub> (98%, ThermoFisher and 68%, BDH Chemicals, respectively) acid mixed at 40 °C for 20 h. The acid mixture containing SWCNTs was diluted by 20× in deionized water. SWCNTs were sedimented overnight. The supernatant was decanted and remaining SWCNTs were washed subsequently with deionized water until neutralization. US-SWCNTs-BSA dispersions were made with the same process that was followed to prepare short-SWCNTs-BSA dispersions.

#### **SWCNT dispersion characterization**

UV-vis-NIR absorbance spectroscopy. To quantitatively determine the SWCNT concentration and qualitatively assess dispersion quality, SWCNT dispersions were examined using UV-vis-NIR absorbance spectroscopy (Varian Cary 5000 spectrophotometer). Concentration was determined using an extinction coefficient of 2.6 (absorbance mL) (mg mm)<sup>-1</sup> at 930 nm.<sup>32</sup> The stability of long-, short-, and US-SWCNTs-BSA dispersion in both cell culture media at 37 °C and phosphate buffer at pH 5 was monitored over 3 days using absorbance spectroscopy by quantifying the peak width at half max of the van Hove peaks in the NIR region (Fig. S1, ESI†). Stability of SWCNTs-BSA in ultrapure deionized water has been reported previously.1,2 The absorbance spectra of long- and short-SWCNTs-BSA also show sharp van Hove peaks that are indicative of individually dispersed SWCNTs. The peaks in the absorbance spectra of US-SWCNTs-BSA are less pronounced likely due to chemical

functionalization of SWCNT surfaces during acid-based length shortening.

Raman spectroscopy. The SWCNT structure after dispersion and the dispersion state in suspension were characterized using Raman spectroscopy. Samples diluted to  $\sim 0.1$  absorbance cm<sup>-1</sup> in water were analyzed on an inverted, inVia confocal Raman microscope (Renishaw) using a 50× air objective with a 0.75 numerical aperture (NA) and a 785 nm laser (i.e., E<sub>laser</sub> = 1.58 eV; 100 mW). Spectra were acquired between 100-3200 cm<sup>-1</sup> (Fig. S2A, ESI†). Each Raman spectrum was normalized to its G-band intensity. Note that the G-band is a characteristic Raman feature of SWCNTs and quantifies the sp2-hybridized carbon bonds in the samples. The D-band-to-G-band intensity ratio  $(I_D:I_G)$  was calculated by dividing the D-band intensity at  $\sim 1300 \text{ cm}^{-1}$  by the G-band intensity at  $\sim 1590 \text{ cm}^{-1}$ ; note that the D-band characterizes the sp<sup>3</sup>-hybridized carbon in the samples. For the G-band, spectra between 1188-1696 cm<sup>-1</sup> (centered at 1450 cm<sup>-1</sup>) were collected with 0.88 cm<sup>-1</sup> resolution. Spectra between 100-650 cm<sup>-1</sup> (centered at 350 cm<sup>-1</sup>), which include radial breathing modes (RBMs) spanning 200-280 cm<sup>-1</sup> that are sensitive to the aggregation state of SWCNTs, were collected with 1.08 cm<sup>-1</sup> resolution. The bundle fraction of each dispersion was quantified by normalizing the maximum RBM intensity >250 cm<sup>-1</sup> by the sum of maximum RBM intensities between 200-250 cm<sup>-1</sup> and 250-275 cm<sup>-1</sup> (Fig. S2B, ESI†).<sup>44</sup> For NIR fluorescence, spectra between 2238–2659 cm<sup>-1</sup> (centered at 2450 cm<sup>-1</sup>) were collected with 0.71 cm<sup>-1</sup> resolution. The NIR fluorescence intensity of each sample was obtained by integrating the signal between 2250-2650 cm<sup>-1</sup> normalized by its G-band intensity (Fig. S2C, ESI†).

A small  $I_{\rm D}$ : $I_{\rm G}$  of 0.03–0.09 of the Raman spectra of SWCNT dispersions confirms that the SWCNT structure remains largely intact through the dispersion process (Fig. S2A, ESI†). The RBMs, magnified in the left panel, show that US-SWCNTs-BSA do not possess some of the chiralities that are present in long-and short-SWCNTs-BSA possibly lost during acid-based length shortening. All SWCNTs-BSA dispersions have significantly lower bundle fractions than the SWCNT powder (\*\*\*p < 0.001) (Fig. S2A, ESI†). Long-SWCNTs-BSA dispersions contain a significantly higher bundle fraction than short- and US-SWCNTs-BSA (\*\*p < 0.01), which is likely a result of the gentle dispersion technique utilized to retain longer length SWCNTs.

The broad peaks over 1100–3100 cm $^{-1}$  result from SWCNT fluorescence (Fig. S2A, ESI†). The NIR fluorescence intensity was calculated from the integrated intensity between 2250–2650 cm $^{-1}$  and then normalized to the G-band intensity (Fig. S2C, ESI†). Both short- and long-SWCNTs-BSA dispersions (\*\*p < 0.01) provide significantly greater NIR fluorescence than the SWCNT powder and US-SWCNTs-BSA (\*\*p < 0.01). Long-SWCNTs-BSA dispersions show a greater NIR fluorescence intensity compared to short-SWCNTs-BSA despite possessing a greater bundle fraction. US-SWCNTs-BSA dispersions display comparably low NIR fluorescence likely because quantum yield of SWCNTs decreases with length shortening.

Quantum yield. We estimated lengths and length variations of the long- and US-SWCNTs by measuring quantum yield of

long-, short-, and US-SWCNTs-BSA dispersions using an NIR fluorescence spectrometer (Nanolog, Horiba Jobin Yvon). Long-SWCNTs-BSA have significantly greater quantum yield than short- and US-SWCNTs-BSA (\*\*p < 0.01), suggesting a longer average length (Fig. S3, ESI†). US-SWCNTs-BSA display the lowest quantum yield. The lengths and length variations of the long- and US-SWCNTs were then estimated from the relative quantum yield using the relationship: quantum yield  $\propto$  (SWCNT length)² (Fig. S3B, ESI†). The length and length variation of length-fractionated short-SWCNTs (145  $\pm$  17 nm), which had been previously determined, was used as a reference.  $^{21,37,39,41}$ 

#### Cell culture and treatment

J774A.1 mouse macrophage-like cells (ATCC) were cultured in Dulbecco's Modified Eagle's Medium (DMEM, 4500 mg  $\rm L^{-1}$  glucose, 4.0 mM  $\rm L\textsc{-}glutamine$ , without sodium pyruvate, ThermoFisher, Hyclone), supplemented with 10% v/v fetal bovine serum (FBS, ThermoFisher) and 1% v/v penicillinstreptomycin (P/S, ThermoFisher). NIH-3T3 mouse fibroblast cells (ATCC) were cultured in a similar medium, except with newborn calf serum (CS, ThermoFisher) instead of FBS. Cells were maintained at 37 °C and 5% CO2.

SWCNT uptake per cell. For bulk uptake measurements, macrophage and fibroblast cells were seeded at 2  $\times$  10<sup>4</sup> and  $3 \times 10^4$  cells cm<sup>-2</sup> into 24-well plates, respectively, and maintained in culture for 24 h. For cell-type dependent uptake, short-SWCNTs-BSA were diluted to a final concentration of 30 µg mL<sup>-1</sup> in a fresh medium, and both macrophages and fibroblasts were exposed for 24 h and 48 h. For lengthdependent uptake, long, short-, and US-SWCNTs-BSA were diluted to a final concentration of 30 µg mL<sup>-1</sup> in a fresh medium and macrophages were exposed for 24 h and 48 h. Each treatment was performed in duplicate. The exposure medium was removed and cells were gently washed once in PBS. A fresh medium was added and cells were labelled with Hoechst 33342 and propidium iodide (PI) for quantification of proliferation and viability. Images were taken for  $\geq 5$  fields of view of ~0.4 mm<sup>2</sup> each on a Leica DMI 6000B inverted light and fluorescence microscope maintained at 37 °C with a 20× (0.4 NA) air objective. Nuclei were segmented and counted in ImageI, and the average cell density was extrapolated to determine the cells per well for uptake normalization. Cell viability and proliferation of macrophages upon uptake of long-, short-, and US-SWCNTs-BSA were determined from percentages of PI(+) cells and the number of cells relative to the control, respectively. Macrophages do not show a significant decrease in viability for all three SWCNT lengths (Fig. S4A, ESI†). However, they show the lowest proliferation after uptake of long-SWCNTs-BSA for 48 h (Fig. S4B, ESI†) and this property is consistent with previous report.5

SWCNT subcellular imaging. For subcellular Raman mapping measurements, macrophage and fibroblast cells were seeded at  $1 \times 10^4$  and  $3 \times 10^4$  cells cm $^{-2}$  onto sterilized #1.5 coverslips, respectively, and maintained in culture for 24 h. For cell-type dependent processing and recovery comparisons in fibroblasts and macrophages, short-SWCNTs-BSA were diluted to a final

concentration of 30 µg mL<sup>-1</sup> in a fresh medium and cells were exposed for 24 h followed by recovery. We also performed an identical set of experiments with 10 µg mL<sup>-1</sup> short-SWCNTs-BSA because at a lower SWCNT concentration, it is easier to discern correlation between the intercellular SWCNT retention and SWCNT dispersion state. For length-dependent recovery comparisons in macrophages, long-, short-, and US-SWCNTs-BSA were diluted to a final concentration of 30 ug mL<sup>-1</sup> in a fresh medium and cells were exposed for 24 h followed by recovery. For recovery conditions, the treatment medium was removed, exchanged for a fresh medium without SWCNTs, and cells were maintained in culture for an additional 24 h. At the completion of cell recovery, the medium was removed and cells were washed 3× in PBS and fixed with 3.7% v/v formaldehyde (Sigma-Aldrich) for 15 min and mounted onto glass slides.

#### Quantification of SWCNT uptake

Cells were lysed using a combination of Triton X-100 and one freeze thaw cycle and were probe-tip sonicated for  $\sim 10$  s at 6 W (Fisher Scientific, Model 100; 3 mm tip diameter). Cellular solutions were then pipetted into 24-well MatTek #1.5 glass bottom plates and subjected to confocal Raman spectroscopy. The SWCNT concentration was determined from the G-band intensity above the baseline using a standard concentration curve that relates the G-band intensity to the SWCNT concentration determined via UV-vis-NIR absorbance spectroscopy for long-, short-, and US-SWCNTs-BSA (Fig. S5A, ESI†).

#### Phase contrast and subcellular Raman imaging

Phase contrast imaging and Raman spectroscopy mapping were performed on an inverted, inVia confocal Raman microscope (Renishaw) using a 0.9 NA air condenser and a 100× (1.4 NA) oil immersion objective. For Raman mapping, a 785 nm laser (100 mW) was used as the light source. Control of mapping parameters and image processing were performed using WiRE software (Renishaw). For Raman mapping, Raman spectra were acquired with an X-Y step size  $\leq$  3.0  $\mu$ m for one field of view. Excitation laser power of 5% was used to prevent sample degradation and ensure accurate bundle fraction quantification. Spectra corresponding to the G-band, RBMs, and NIR fluorescence region were taken sequentially over the same X-Y coordinates all with an integration time of 2 s.

#### Spatial maps and quantification

Spatial maps of the G-band intensity, bundle fraction, and NIR fluorescence were performed in MATLAB (MathWorks). The maximum G-band intensity between 1540-1610 cm maximum individual RBM intensity between 200-250 cm<sup>-1</sup>, and maximum bundle RBM intensity between 250-275 cm<sup>-1</sup> above the baseline in the respective regions were calculated for each data pixel. For NIR fluorescence, the integrated area under the spectral curve between 2250-2650 cm<sup>-1</sup> was tabulated. The bundle fraction was quantified by normalizing the maximum bundle RBM intensity by the sum of maximum individual and maximum bundle RBM intensities.44 NIR fluorescence was quantified by normalizing the integrated area by the maximum

G-band intensity. The local SWCNT concentration was determined using a calibration curve relating the G-band intensity to the SWCNT concentration determined via UV-vis-NIR absorbance spectroscopy for long-, short-, and US-SWCNTs-BSA (Fig. S5B, ESI†). Spectra with a G-band signal-to-noise ratio of < 3 were excluded from the analysis. Subcellular phase dense regions of interest were manually segmented in ImageJ and the corresponding individual and bundle RBM intensities within the segmented region were quantified. Statistical analysis between indicated samples was performed by unpaired Student's t-test.

## Results

#### Macrophages retain SWCNTs more than fibroblasts

Under conditions that we have previously established for optimal cell delivery of short-SWCNTs-BSA, 32 we exposed both macrophages and fibroblasts to 30 μg mL<sup>-1</sup> short-SWCNTs-BSA for 24 h and then imaged SWCNT uptake, intracellular distribution, and recovery using the G-band Raman signal. We chose the final exposure concentration of SWCNTs to be 30 μg mL<sup>-1</sup> for our experiments since this is the threshold concentration where the rate of SWCNTs-BSA uptake in fibroblasts reaches a steady state.<sup>32</sup> For macrophages, this is the threshold concentration

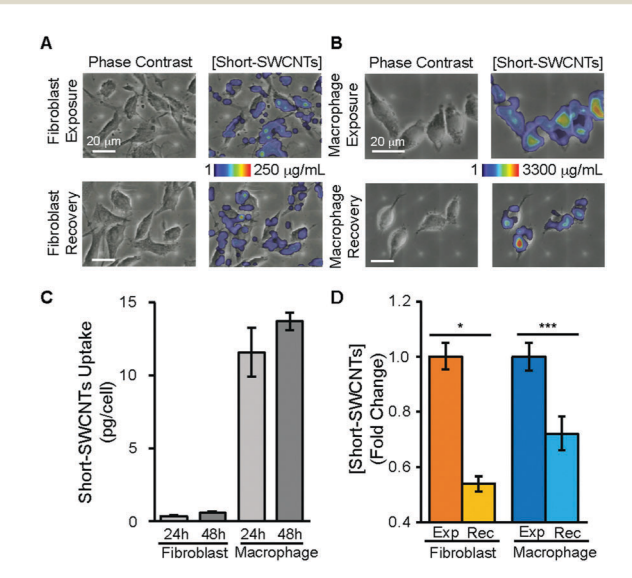


Fig. 1 Uptake and recovery of short-SWCNTs-BSA into fibroblasts and macrophages. (A) Co-localized phase contrast and confocal Raman images of the G-band show short-SWCNTs-BSA localization within fibroblasts exposed to 30  $\mu g \ mL^{-1}$  for 24 h (exposure) followed by 24 h in a SWCNT-free medium (recovery). (B) Similar conditions for macrophages show that the maximum short-SWCNTs-BSA uptake is nearly an order of magnitude higher with more punctate distribution within cells upon both exposure and in recovery. Scale bars reflect 20 µm. (C) Average mass of short-SWCNTs internalized per cell for 2 cm<sup>2</sup> quantified using Raman spectroscopy shows higher uptake for macrophages compared to fibroblasts, particularly at 30  $\mu g$  mL<sup>-1</sup> exposure. Data = mean  $\pm$  SEM,  $n \ge 2$ replicate experiments. (D) Setting the exposure data to 1.0, we calculated the recovery levels to a fraction of the maximum levels for fibroblast and macrophage; \*p < 0.05; \*\*\*p < 0.001. Data = mean  $\pm$  SEM,  $n \ge 630$ (320) and 560 (290) voxels for exposure (recovery) for fibroblasts and macrophages, respectively.

for short-SWCNTs-BSA before cells undergo drastic changes in shape, as we have previously reported.11 In parallel, to determine recovery of cells from SWCNT exposure, we also exposed both cell types to 30  $\mu g\ mL^{-1}$  of short-SWCNTs-BSA for 24 h followed by 24 h with no exposure to SWCNTs. Note that the recovery is a function of both expulsion of SWCNTs and cell division, and that the doubling time of J774A.1 and NIH-3T3 cells is similar ( $\sim$ 20 h). Consistent with previous reports, <sup>11,32</sup> macrophages take up more short-SWCNTs-BSA than fibroblasts at 30  $\mu$ g mL<sup>-1</sup> exposure for both 24 h and 48 h (Fig. 1B and C). In addition, macrophages retain significantly higher levels of short-SWCNTs-BSA after a 24 h recovery period compared to fibroblasts (Fig. 1D). Spatial imaging of the recovered fibroblasts (Fig. 1A) and macrophages (Fig. 1B) shows differential subcellular localization patterns for SWCNTs. Recovered fibroblasts have lower levels of uniform G-band intensity over the entire cell (Fig. 1A, recovery) indicating that a large percentage of SWCNTs is exocytosed. In contrast, macrophages maintain a heterogeneous distribution of the SWCNT concentration with distinct, intense regions (Fig. 1B, recovery). Since macrophages are professional phagocytes and fibroblasts take in materials primarily through endocytosis, differential distributions within cells are expected.

#### SWCNT retention correlates with bundling

To determine if cell-specific processes affect the dispersion state of short-SWCNTs-BSA after uptake and in turn their expulsion from cells, we performed Raman scans of each confocal voxel within cells to determine the total concentration of SWCNTs (G-band intensity at 1590 cm<sup>-1</sup>), bundled SWCNTs  $(RBMs > 250 \text{ cm}^{-1})$ , and individualized SWCNTs (NIR fluorescence between 2250-2650 cm<sup>-1</sup>). Ideally, SWCNTs should either be individualized or bundled within cells, so the bundling

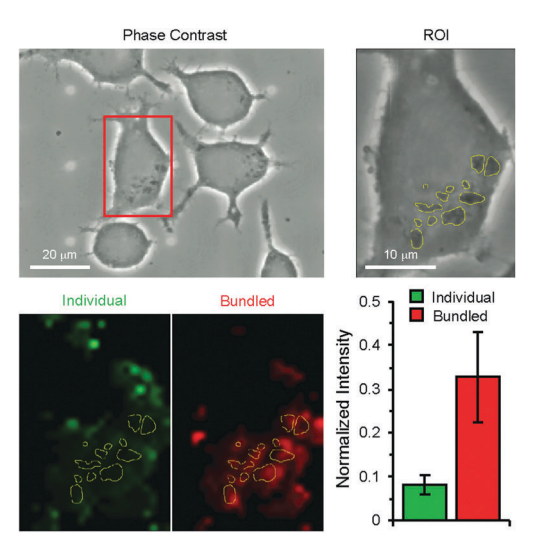


Fig. 2 Intracellular distribution and dispersion state of short-SWCNTs-BSA in macrophages after 10 µg mL<sup>-1</sup> exposure for 24 h. Spatial correlation of phase dense subcellular regions identified in phase contrast images with Raman spectroscopy mapping results shows that these regions are preferentially comprised of less individual and more bundled SWCNTs. Data = mean  $\pm$  SD.

fraction should go inversely with the NIR fluorescence intensity. High resolution phase contrast imaging of short-SWCNTs-BSA treated macrophages exposed to a concentration of 10 µg mL<sup>-1</sup> shows a distinct subcellular distribution of individual and bundled SWCNTs (Fig. 2). The phase dense punctate regions with a high concentration of bundled SWCNTs are best observed at this concentration. At 30  $\mu g$  mL<sup>-1</sup>, the phase dense regions are widely distributed in a cell with overlapped areas of individual and bundled SWCNTs because cells uptake a high amount of SWCNTs (Fig. S6, ESI†). Furthermore, Raman spectra based imaging of short-SWCNTs-BSA shows that SWCNTs are highly bundled within the phase-dense regions. In contrast, SWCNTs remain largely unbundled in the fibroblasts (Fig. 3A). The average NIR fluorescence intensity is also higher in fibroblasts versus in macrophages (Fig. 3B and Fig. S7, ESI†), corroborating higher SWCNT bundling in macrophages. Interestingly, the low degree of bundling after exposure is similar to that after recovery for fibroblasts but decreases slightly for macrophages (Fig. 3A), although the NIR fluorescence intensity after recovery increases minimally for fibroblasts and noticeably for macrophages (Fig. 3B). This could be due to a small fraction of bundles (less than 10%) being processed and individualized within the cell

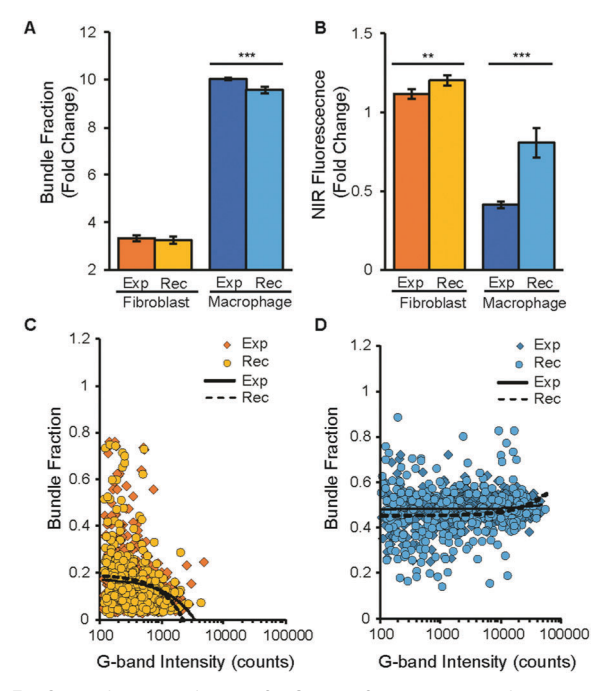


Fig. 3 Quantification of short-SWCNTs-BSA bundling in fibroblasts and macrophages. (A) Quantification of the bundle fraction from RBMs shows lower bundling in fibroblasts than macrophages in both exposure (Exp) and recovery (Rec); \*\*\*p < 0.001. (B) Corresponding NIR fluorescence signal from individualized SWCNTs is higher in fibroblasts compared with macrophages. Fold change quantifications in cells are relative to the starting value of short-SWCNTs-BSA dispersion; \*\*p < 0.01; \*\*\*p < 0.001. (C) In fibroblasts, comparison of bundling with the G-band intensity for every imaged voxel shows that bundling is dependent of the G-band intensity for both exposure and in recovery. (D) In macrophages, bundling is independent of short-SWCNTs-BSA concentration for both exposure and recovery. Data = mean  $\pm$  SEM,  $n \ge 630$  (320) and 560 (290) voxels for exposure (recovery) for fibroblasts and macrophages, respectively.

during the recovery time, which in sum is on the order of two cell division cycles (24 hour for exposure and 24 hour for recovery).

Since it is plausible that the higher uptake of SWCNTs in macrophages relative to that in fibroblasts may lead to more bundling in macrophages, we simultaneously imaged bundling with the G-band intensity (Fig. 3C and D and Fig. S8, ESI†). We find that for macrophages bundling is largely independent of the G-band intensity, both for exposure and recovery (Fig. 3D). Interestingly, fibroblasts show bundling to be dependent on the concentration for exposure and recovery, showing that a larger intracellular short-SWCNT concentration is associated with decreased bundling. This suggests that less intense regions are more likely to be bundled (Fig. 3C). Thus, similar to recovery (Fig. 1A), short-SWCNTs-BSA appear to diffuse subcellularly and less bundled in fibroblasts, likely enabling these cells to expel SWCNTs (Fig. 1A) compared to highly bundled SWCNTs in macrophages, which are largely retained (Fig. 1B).

### SWCNT uptake is a function of length, but bundling and retention are more complex

The uptake of SWCNTs-BSA in macrophages is a strong function of SWCNT length (Fig. 4 and 5A) and is consistent with previous observations. 2,32 Long-SWCNTs with large length polydispersity show the lowest delivery to cells and we suggest that much of the macrophage uptake is from shorter length SWCNTs within the distribution. Uptake is slightly higher for short-SWCNTs, which have a much narrower length distribution, and is drastically higher for US-SWCNTs (Fig. 5A). However, SWCNT bundling after cellular uptake does not follow the same trend. Short-SWCNTs become highly bundled but US-SWCNTs and long-SWCNTs remain mostly individualized as evidenced by a lower bundle fraction (Fig. 4 and 5C and Fig. S9A, ESI†) and a higher NIR fluorescence intensity (Fig. 4 and 5D and Fig. S9B, ESI†).

Since macrophage entry mechanisms of US- and short-SWCNTs are likely similar and the SWCNT dispersion state is

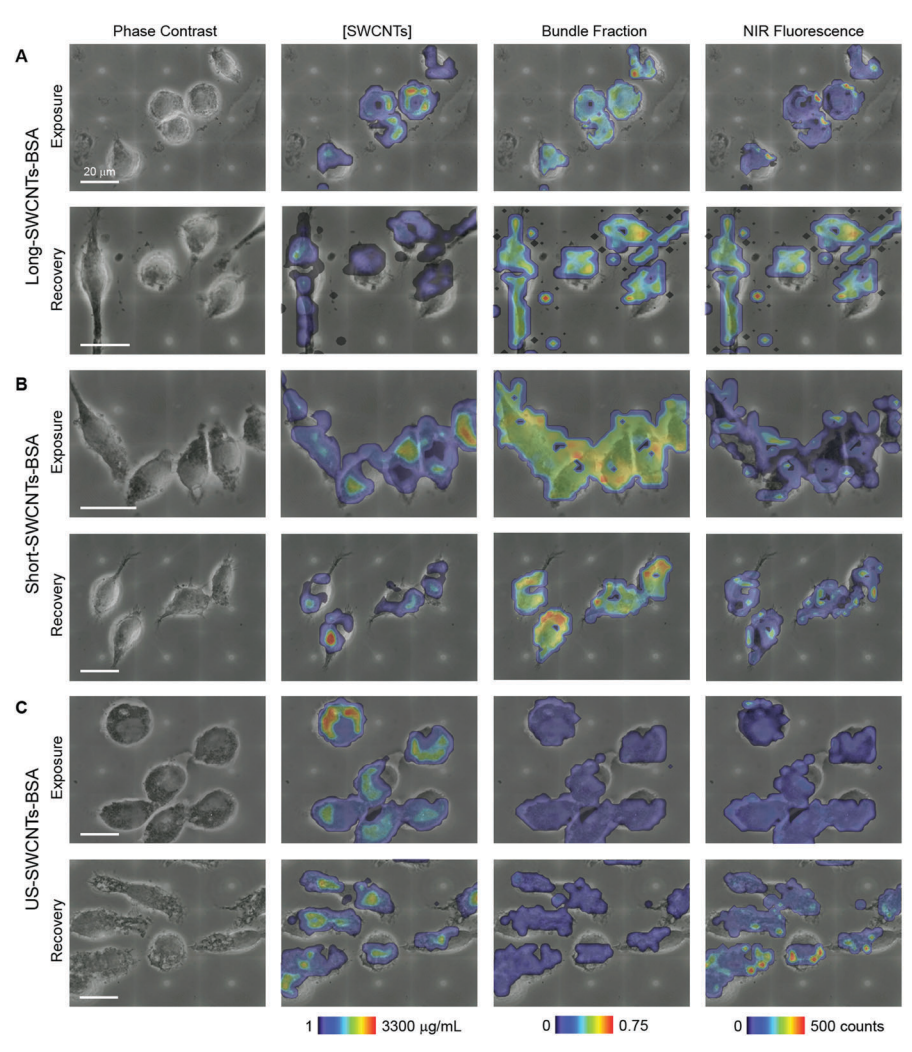


Fig. 4 Differential uptake and bundling of (A) long-, (B) short- and (C) US-SWCNTs-BSA in macrophages. Raman spectroscopy maps taken over individual cells. Each pixel represents a Raman spectrum containing the G-band signal for SWCNT concentration as well as processed RBM and NIR fluorescence intensities used to quantify the SWCNT dispersion state. US-SWCNTs-BSA show highest uptake, but short-SWCNTs-BSA show highest bundling. Scale bars reflect 20 µm.

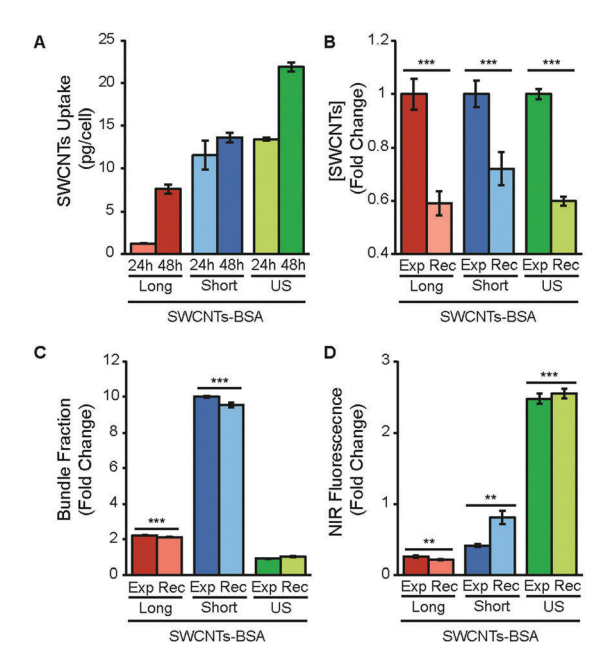


Fig. 5 Uptake, concentrations and bundling of long-, short- and US-SWCNTs-BSA in macrophages after exposure and recovery. (A) Uptake of 30  $\mu$ g mL<sup>-1</sup> SWCNTs at 24 h and 48 h for 2 cm<sup>2</sup> culture area. Data = mean  $\pm$  SEM,  $n \ge 2$  replicate experiments. (B) Setting the exposure data to 1.0, we calculated the recovery levels to a fraction of the maximum levels. Significantly more long- and US-SWCNTs-BSA are lost from macrophages compared to short-SWCNTs-BSA despite higher uptake levels (cf. Fig. 4); \*\*\*p < 0.001. (C) Bundling fraction calculated from RBMs and (D) individualized SWCNTs from NIR fluorescence both suggest that US-SWCNTs-BSA are less bundled in cells than short-SWCNTs-BSA; \*\*p < 0.01; \*\*\*p < 0.001. Fold change quantification for SWCNTs in cells relative to their respective starting values as dispersions in solution. Data = mean  $\pm$  SEM,  $n \ge 460$  (350), 560 (290), and 530 (450) voxels for exposure (recovery) for long-, short-, and US-SWCNTs-BSA, respectively.

possibly an outcome of length-dependent cellular processing, we investigated the recovery of macrophages after exposure to long-, short- and US-SWCNTs (Fig. 4 and 5). Macrophages retain significantly low levels of US-SWCNTs compared with short-SWCNTs (Fig. 5B). This low retention correlates with the high percentage of individual SWCNTs (low bundling (Fig. 4 and 5C) and high NIR fluorescence intensity after recovery (Fig. 4 and 5D)) observed before and after recovery.

## Discussion

#### Delivery versus retention in cells

Delivery of SWCNTs into cells has been widely studied through measuring uptake. However, for cellular therapies with SWCNTs ultimate delivery is a function of increased cellular internalization as well as retention. Differential coatings on SWCNTs often lead to altered cellular uptake, subcellular localization and ultimately disparate retention patterns.<sup>2,33,46</sup> Furthermore, different cell types can uptake and process materials in different ways leading to altered retention.1 In addition to the studies here, others have seen that macrophages and other phagocytes

take in and retain SWCNTs more than fibroblasts and epithelial cells. 21,22 In this work, we observe that the high uptake associated with BSA coatings combined with length-dependent intracellular bundling contribute to the retention of large amounts of SWCNTs in macrophages.

### Potential mechanism for length-dependent SWCNT bundling

Uptake is size-dependent with uptake of US-SWCNTs is higher than that of short-SWCNTs, which is higher than that of long-SWCNTs. However, neither long- nor US-SWCNTs bundle appreciably inside cells, especially compared to the high fraction of bundling displayed for short-SWCNTs. We suggest that long-SWCNTs are processed slowly inside of cells because of their large size. Combined with low uptake, long-SWCNTs manage to avoid bundling. In comparison, macrophages possibly can readily take in and process US-SWCNTs and short-SWCNTs very likely via similar uptake mechanisms. Short-SWCNTs are collected and compressed in vacuoles, probably phagosomes (Fig. 2), where SWCNTs bundle due to the lateral attraction from van der Waals forces overcoming entropic fluctuations. In contrast, US-SWCNTs likely evade bundling inside these vacuoles because entropic fluctuations are significantly larger relative to lateral attraction.

#### Cell mediated SWCNT delivery

While high levels of delivered SWCNTs (uptake plus retention) may be preferential for many biomedical applications, there are also applications associated with controlled release. The high loading of US-SWCNTs into macrophages and subsequent slow release may be of interest for cell-mediated delivery of SWCNTs to other target cells. Macrophages could serve as efficient SWCNT carriers since they intrinsically traffic materials to regions not easily accessible with traditional delivery strategies, including the blood-brain barrier<sup>47</sup> and to hypoxic regions in tumors. 48 There are other applications such as macrophages "leaving trails of breadcrumbs" for imaging of macrophage movements within tissues. These potential applications are exciting, but require multiple cell types as well as tissue-level in vivo examination.

## Conclusions

We have determined the dependence of cellular processing including uptake, subcellular distribution, and retention on the SWCNT length and immune cell-specific processes. As expected, macrophages uptake larger amounts of SWCNTs than fibroblasts. Surprisingly, short-SWCNTs became highly bundled while US- and long-SWCNTs remained individualized in macrophages. Furthermore, short-SWCNTs do not bundle in fibroblasts. These bundled short-SWCNTs are retained in macrophages, whereas unbundled SWCNTs are lost from fibroblasts. US-SWCNTs and long-SWCNTs are also lost from macrophages after 24 h of recovery. Thus, SWCNT length appears to play a critical role in the dispersion state of SWCNTs after intracellular processing

Paper

by immune cells, ultimately influencing the retention and expulsion of SWCNTs by cells over time.

## Acknowledgements

We thank B. D. Holt for useful discussion. This work was supported by the National Science Foundation through grants CMMI-1335417 (M. F. I.) and CMMI-1634888 (K. N. D.).

## Notes and references

- 1 B. D. Holt, K. N. Dahl and M. F. Islam, *Small*, 2011, 7, 2348–2355.
- 2 B. D. Holt, J. J. Law, P. D. Boyer, L. J. Wilson, K. N. Dahl and M. F. Islam, *ACS Appl. Mater. Interfaces*, 2015, 7, 14593–14602.
- 3 B. S. Wong, S. L. Yoong, A. Jagusiak, T. Panczyk, H. K. Ho, W. H. Ang and G. Pastorin, *Adv. Drug Delivery Rev.*, 2013, **65**, 1964–2015.
- 4 L. Rajendran, H.-J. Knolker and K. Simons, *Nat. Rev. Drug Discovery*, 2010, **9**, 29–42.
- 5 R. Foldbjerg, E. S. Irving, J. Wang, K. Thorsen, D. S. Sutherland, H. Autrupa and C. Beer, *Toxicol. Res.*, 2014, 3, 228–241.
- 6 K. Kostarelos, L. Lacerda, G. Pastorin, W. Wu, S. Wieckowski, J. Luangsivilay, S. Godefroy, D. Pantarotto, J. P. Briand, S. Muller, M. Prato and A. Bianco, *Nat. Nanotechnol.*, 2007, 2, 108–113.
- 7 F. Chellat, Y. Merhi, A. Moreau and L. Yahia, *Biomaterials*, 2005, 26, 7260-7275.
- 8 D. M. Mosser and J. P. Edwards, *Nat. Rev. Immunol.*, 2008, 8, 958–969.
- 9 A. Battigelli, C. Menard-Moyon and A. Bianco, *J. Mater. Chem. B*, 2014, 2, 6144–6156.
- 10 T. R. Fadel and T. M. Fahmy, *Trends Biotechnol.*, 2014, 32, 198–209.
- 11 P. D. Boyer, B. D. Holt, M. F. Islam and K. N. Dahl, *Soft Matter*, 2013, **9**, 758–764.
- 12 H. Dumortier, S. Lacotte, G. Pastorin, R. Marega, W. Wu, D. Bonifazi, J. P. Briand, M. Prato, S. Muller and A. Bianco, *Nano Lett.*, 2006, 6, 1522–1528.
- 13 V. E. Kagan, Y. Y. Tyurina, V. A. Tyurin, N. V. Konduru, A. I. Potapovich, A. N. Osipov, E. R. Kisin, D. Schwegler-Berry, R. Mercer, V. Castranova and A. A. Shvedova, *Toxicol. Lett.*, 2006, 165, 88–100.
- 14 Z. Liu, C. Davis, W. B. Cai, L. He, X. Y. Chen and H. J. Dai, *Proc. Natl. Acad. Sci. U. S. A.*, 2008, **105**, 1410–1415.
- 15 M. L. Schipper, N. Nakayama-Ratchford, C. R. Davis, N. W. S. Kam, P. Chu, Z. Liu, X. M. Sun, H. J. Dai and S. S. Gambhir, *Nat. Nanotechnol.*, 2008, 3, 216–221.
- 16 I. A. Khalil, K. Kogure, H. Akita and H. Harashima, *Pharma-col. Rev.*, 2006, 58, 32–45.
- 17 G. Sahay, D. Y. Alakhova and A. V. Kabanov, *J. Controlled Release*, 2010, **145**, 182–195.

- 18 P. X. Dong, B. Wan and L. H. Guo, *Nanotoxicology*, 2012, 6, 288–303.
- 19 P. X. Dong, B. Wan, Z. X. Wang, L. H. Guo, Y. Yang and L. X. Zhao, *Nanotoxicology*, 2013, 7, 1028–1042.
- 20 B. Wan, Z. X. Wang, Q. Y. Lv, P. X. Dong, L. X. Zhao, Y. Yang and L. H. Guo, *Toxicol. Lett.*, 2013, 221, 118–127.
- 21 M. L. Becker, J. A. Fagan, N. D. Gallant, B. J. Bauer, V. Bajpai, E. K. Hobbie, S. H. Lacerda, K. B. Migler and J. P. Jakupciak, *Adv. Mater.*, 2007, **19**, 939–945.
- 22 D. A. Donkor and X. W. S. Tang, *Biomaterials*, 2014, 35, 3121–3131.
- 23 H. Jin, D. A. Heller, R. Sharma and M. S. Strano, ACS Nano, 2009, 3, 149–158.
- 24 B. Kang, S. Q. Chang, Y. D. Dai, D. C. Yu and D. Chen, *Small*, 2010, **6**, 2362–2366.
- 25 J. Rejman, V. Oberle, I. S. Zuhorn and D. Hoekstra, *Biochem. J.*, 2004, 377, 159–169.
- 26 J. Kolosnjaj-Tabi, K. B. Hartman, S. Boudjemaa, J. S. Ananta, G. Morgant, H. Szwarc, L. J. Wilson and F. Moussa, ACS Nano, 2010, 4, 1481–1492.
- 27 V. Raffa, G. Ciofani, O. Vittorio, C. Riggio and A. Cuschieri, Nanomedicine, 2010, 5, 89–97.
- 28 G. Jia, H. Wang, L. Yan, X. Wang, R. Pei, T. Yan, Y. Zhao and X. Guo, *Environ. Sci. Technol.*, 2005, 39, 1378–1383.
- 29 E. Witasp, A. A. Shvedova, V. E. Kagan and B. Fadeel, *Inhalation Toxicol.*, 2009, 21(suppl 1), 131–136.
- 30 P. Cherukuri, S. M. Bachilo, S. H. Litovsky and R. B. Weisman, *J. Am. Chem. Soc.*, 2004, **126**, 15638–15639.
- 31 D. A. Heller, S. Baik, T. E. Eurell and M. S. Strano, *Adv. Mater.*, 2005, **17**, 2793–2799.
- 32 B. D. Holt, K. N. Dahl and M. F. Islam, *ACS Nano*, 2012, **6**, 3481–3490.
- 33 B. D. Holt, M. C. McCorry, P. D. Boyer, K. N. Dahl and M. F. Islam, *Nanoscale*, 2012, 4, 7425–7434.
- 34 B. D. Holt, V. Roginskaya, B. Van Houten, M. F. Islam and K. N. Dahl, *J. Mater. Chem. B*, 2017, 5, 369–374.
- 35 P. D. Boyer, H. Shams, S. L. Baker, M. R. K. Mofrad, M. F. Islam and K. N. Dahl, *J. Mater. Chem. B*, 2016, 4, 1324–1330.
- 36 D. A. Tsyboulski, Y. Hou, N. Fakhri, S. Ghosh, R. Zhang, S. M. Bachilo, M. Pasquali, L. Chen, J. Liu and R. B. Weisman, *Nano Lett.*, 2009, 9, 3282–3289.
- 37 J. A. Fagan, M. L. Becker, J. Chun and E. K. Hobbie, *Adv. Mater.*, 2008, **20**, 1609–1613.
- 38 M. F. Islam, D. E. Milkie, O. N. Torrens, A. G. Yodh and J. M. Kikkawa, *Phys. Rev. B: Condens. Matter Mater. Phys.*, 2005, 71, 201401.
- 39 M. F. Islam, E. Rojas, D. M. Bergey, A. T. Johnson and A. G. Yodh, *Nano Lett.*, 2003, 3, 269–273.
- 40 D. E. Johnston, M. F. Islam, A. G. Yodh and A. T. Johnson, *Nat. Mater.*, 2005, 4, 589–592.
- 41 M. S. Arnold, A. A. Green, J. F. Hulvat, S. I. Stupp and M. C. Hersam, *Nat. Nanotechnol.*, 2006, **1**, 60–65.
- 42 Y. Y. Huang, T. P. J. Knowles and E. M. Terentjev, *Adv. Mater.*, 2009, **21**, 3945–3948.

- 43 J. Liu, A. G. Rinzler, H. J. Dai, J. H. Hafner, R. K. Bradley, P. J. Boul, A. Lu, T. Iverson, K. Shelimov, C. B. Huffman, F. Rodriguez-Macias, Y. S. Shon, T. R. Lee, D. T. Colbert and R. E. Smalley, *Science*, 1998, 280, 1253–1256.
- 44 D. Yoon, J. B. Choi, C. S. Han, Y. J. Kim and S. Baik, *Carbon*, 2008, **46**, 1530–1534.
- 45 A. Rajan, M. S. Strano, D. A. Heller, T. Hertel and K. Schulten, *J. Phys. Chem. B*, 2008, **112**, 6211–6213.
- 46 B. D. Holt, H. Shams, T. A. Horst, S. Basu, A. D. Rape, Y.-L. Wang, G. K. Rohde, M. R. K. Mofrad, M. F. Islam and K. N. Dahl, J. Funct. Biomater., 2012, 3, 398–417.
- 47 S. Madsen, S.-K. Baek, A. Makkouk, T. Krasieva and H. Hirschberg, *Ann. Biomed. Eng.*, 2012, **40**, 507–515.
- 48 M.-R. Choi, K. J. Stanton-Maxey, J. K. Stanley, C. S. Levin, R. Bardhan, D. Akin, S. Badve, J. Sturgis, J. P. Robinson, R. Bashir, N. J. Halas and S. E. Clare, *Nano Lett.*, 2007, 7, 3759–3765.